Available online at www.sciencedirect.com
SCIENCE DIRECT®
Journal of Organometallic Chemistry 690 (2005) 1178–1191
Journal of Organometallic Chemistry
www.elsevier.com/locate/jorganchem

Synthesis, characterization and Schlenk equilibrium studies of methylmagnesium compounds with *O*- and *N*-donor ligands – the unexpected behavior of [MgMeBr(pmdta)] (pmdta = *N*,*N*,*N*′,*N*″,*N*″-pentamethyldiethylenetriamine)

Rushdi I. Yousef [a], Bernhard Walfort [b], Tobias Rüffer [b], Christoph Wagner [a], Harry Schmidt [a], Renate Herzog [a], Dirk Steinborn [a,*]

[a] *Institut für Anorganische Chemie, Martin-Luther-Universität Halle-Wittenberg, Kurt-Mothes-Straße 2, 06120 Halle/Saale, Germany*
[b] *Institut für Chemie, Technische Universität Chemnitz, Straße der Nationen 62, 09107 Chemnitz, Germany*

Received 23 September 2004; accepted 28 October 2004
Available online 7 February 2005

Abstract

$MgMe_2$ (**1**) was found to react with 1,4-diazabicyclo[2.2.2]octane (dabco) in tetrahydrofuran (thf) yielding a binuclear complex [{$MgMe_2$(thf)}$_2$(μ-dabco)] (**2**). Furthermore, from reactions of MgMeBr with diglyme (diethylene glycol dimethyl ether), NEt_3, and tmeda (*N*,*N*,*N*′,*N*′-tetramethylethylenediamine) in etheral solvents compounds MgMeBr(L), (L = diglyme (**5**); NEt_3 (**6**); tmeda (**7**)) were obtained as highly air- and moisture-sensitive white powders. From a thf solution of **7** crystals of [MgMeBr(thf)(tmeda)] (**8**) were obtained. Reactions of MgMeBr with pmdta (*N*,*N*,*N*′,*N*″,*N*″-pentamethyldiethylenetriamine) in thf resulted in formation of [MgMeBr(pmdta)] (**9**) in nearly quantitative yield. On the other hand, the same reaction in diethyl ether gave MgMeBr(pmdta) · $MgBr_2$(pmdta) (**10**) and [{$MgMe_2$(pmdta)}$_7${MgMeBr(pmdta)}] (**11**) in 24% and 2% yield, respectively, as well as [$MgMe_2$(pmdta)] (**12**) as colorless needle-like crystals in about 26% yield. The synthesized methylmagnesium compounds were characterized by microanalysis and ^{1}H and ^{13}C NMR spectroscopy. The coordination-induced shifts of the ^{1}H and ^{13}C nuclei of the ligands are small; the largest ones were found in the tmeda and pmdta complexes. Single-crystal X-ray diffraction analyses revealed in **2** a tetrahedral environment of the Mg atoms with a bridging dabco ligand and in **8** a trigonal-bipyramidal coordination of the Mg atom. The single-crystal X-ray diffraction analyses of [$MgMe_2$(pmdta)] (**12**) and [$MgBr_2$(pmdta)] (**13**) showed them to be monomeric with five-coordinate Mg atoms. The square-pyramidal coordination polyhedra are built up of three N and two C atoms in **12** and three N and two Br atoms in **13**. The apical positions are occupied by methyl and bromo ligands, respectively. Temperature-dependent ^{1}H NMR spectroscopic measurements (from 27 to −80 °C) of methylmagnesium bromide complexes MgMeBr(L) (L = thf (**4**); diglyme (**5**); NEt_3 (**6**); tmeda (**7**)) in thf-d_8 solutions indicated that the deeper the temperature the more the Schlenk equilibria are shifted to the dimethylmagnesium/dibromomagnesium species. Furthermore, at −80 °C the dimethylmagnesium compounds are predominant in the solutions of Grignard compounds **4**–**6** whereas in the case of the tmeda complex**7** the equilibrium constant was roughly estimated to be 0.25. In contrast, [MgMeBr(pmdta)] (**9**) in thf-d_8 revealed no dismutation into [$MgMe_2$(pmdta)] (**12**) and [$MgBr_2$(pmdta)] (**13**) even up to −100 °C. In accordance with this unexpected behavior, 1:1 mixtures of **12** and **13** were found to react in thf at room temperature yielding quantitatively the corresponding Grignard compound **9**. Moreover, the structures of [MgMeBr(pmdta)] (**9c**), [$MgMe_2$(pmdta)] (**12c**), and [$MgBr_2$(pmdta)] (**13c**) were calculated on the DFT level of theory. The calculated structures **12c** and **13c** are in a good agreement with the experimentally observed structures **12** and **13**. The equilibrium constant of the Schlenk equilibrium (2 **9c** ⇌ **12c** + **13c**) was calculated to be $K_{gas} = 2.0 \times 10^{-3}$ (298 K) in the gas phase. Considering the

* Corresponding author. Tel.: +49 345 55 25620; fax: +49 345 552 7028.
E-mail address: steinborn@chemie.uni-halle.de (D. Steinborn).

0022-328X/$ - see front matter
doi:10.1016/j.jorganchem.2004.10.058

solvent effects of both thf and diethyl ether using a polarized continuum model (PCM) the corresponding equilibrium constants were calculated to be $K_{thf} = 1.2 \times 10^{-3}$ and $K_{ether} = 3.2 \times 10^{-3}$ (298 K), respectively.

Keywords: Methylmagnesium bromide; Dimethylmagnesium; Grignard compounds; Pmdta (*N*,*N*,*N*′,*N*″,*N*″-pentamethyldiethylenetriamine); Schlenk equilibrium; DFT calculations

1. Introduction

For 100 years organomagnesium compounds have been the most important reagents in organic and organometallic synthesis [1–3]. Probably most widely used are Grignard compounds MgRX(L) (**I**, R = alkyl, aryl; X = halide) and diorganomagnesium compounds $MgR_2(L)$ (**II**). Their structures and their reactivities are strongly dependent on the co-ligands L and on the solvents [4]. In 1929, Schlenk and Schlenk Jr. [5] found that the addition of dioxane to etheral solutions of Grignard compounds MgRX (X = halide, R = alkyl, aryl) results in precipitation of magnesium halides. This observation gave proof for the dynamic behavior of Grignard compounds, which is known today as the Schlenk equilibrium. A simple representation of the equilibrium is given in Scheme 1 showing the ''basic'' Schlenk equilibrium (**a**) as well as (schematically) the formation of homo-oligomers (**b/c**) and the hetero-dimer (**d**). Positions of all these equilibria are dependent on the nature of X and R, the concentration, and the temperature. Furthermore, they are critically dependent on the solvent with the generalization that in better coordinating solvents the monomeric species predominate and the position of the Schlenk equilibrium **a** tends to be shifted to the dismutation products [6,7]. In the last years high-level ab initio molecular orbital and density-functional studies provided further insight into the solvation effects on the Schlenk equilibrium [8–11].

Several routes to organomagnesium compounds were reported. The most important ones are the direct oxidative addition of an organic halide to magnesium metal, exchange reactions (metal–hydrogen exchange, metal–halogen exchange), and the addition of a Grignard reagent to an unsaturated bond (carbomagnesiation) [6,7]. The addition of 1,4-dioxane to an etheral Grignard solution, followed by removal of the precipitated dioxane complex of the magnesium dihalide is a common procedure for obtaining MgR_2 [5] although the latter usually contains some residual halogen [3,6]. The second most widely used route to MgR_2 is the exchange reaction between excess magnesium metal and organomercury compounds [12]. The high toxicity of organomercurials is a severe drawback of this method.

The real composition of organomagnesium reagents (especially Grignard compounds **I**) both in solution and in the solid state is far more complex than it is expressed by such simple formula like **I** and **II** [4]. Relatively few information on their solid-state structures [13–15] has been known because in most cases reagents **I** and **II** were used in situ. Thus, even with the most simple organo ligand, i.e. the methyl group, only one ''classical'' Grignard compound was structurally characterized, namely $[MgMeBr(thf)_3]$ having a trigonal-bipyramidal monomeric structure [16]. Furthermore, a tetranuclear complex $[Mg_4Me_2(\mu_2\text{-}Cl)_6(thf)_6]$ that can be considered as a $[MgCl_2(thf)_2]$ adduct of [MgMeCl(thf)] [17] and a trinuclear magnesium amide cluster $[MgI(thf)_5][(MgI)_3(\mu_2\text{-}Me)\{SiMe(N\textit{t}\text{-}Bu)_3\}(thf)]$ [18] having the building block IMg(μ-Me)MgI have been structurally characterized.

In this work, we describe reactions of $MgMe_2$ and MgMeBr with different *O*- and *N*-donors being monodentate (thf, NEt_3), chelating and bridging bidentate (*N*,*N*,*N*′,*N*′-tetramethylethylenediamine, tmeda; 1,4-diazabicyclo[2.2.2]octane, dabco), and tridentate (diethylene glycol dimethyl ether, diglyme; *N*,*N*,*N*′,*N*″,*N*″-pentamethyldiethylenetriamine, pmdta) ligands. Thereby, some novel methylmagnesium complexes were synthesized, isolated in the solid state, and characterized by means of microanalysis, NMR spectroscopy (^1H, ^{13}C), and partially also by single-crystal X-ray diffraction analysis. Furthermore, we studied Schlenk equilibria of some of these Grignard compounds (MgMeBr(L), L = thf, NEt_3, diglyme, tmeda, pmdta) in thf solution as based on ^1H NMR measurements showing that in the case of the pmdta complex the equilibrium lies completely on the side of [MgMeBr(pmdta)]. Further insight into this unexpected behavior was obtained from DFT calculations.

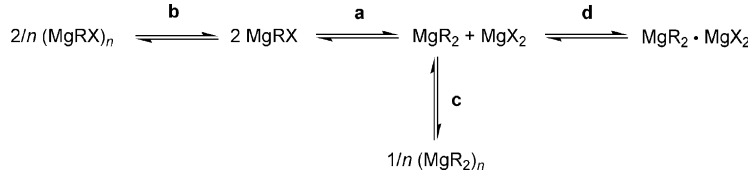

Scheme 1. Schlenk equilibrium (**a**) and formation of associated species (**b**–**d**). For simplicity, solvent molecules are excluded.

2. Results and discussion

2.1. Syntheses

Unsolvated dimethylmagnesium (**1**) was obtained by the well known "dioxane route" [5] from reaction of MgMeBr with 1,4-dioxane in diethyl ether as colorless crystals in 29% yield. The bromine content was determined to be less than 0.2%. Reaction of 1,4-diazabicyclo[2.2.2]octane (dabco) with a twofold excess of **1** in tetrahydrofuran and then cooling down to −40 °C resulted in the formation of [{$MgMe_2$(thf)}$_2$(μ-dabco)] (**2**), a binuclear complex with dabco acting as a bridging ligand. Complex **2** was obtained in 84% yield as colorless highly air- and moisture-sensitive crystals (Scheme 2). Both dimethylmagnesium compounds **1** and **2** were characterized by microanalysis, NMR spectroscopy, and complex **2** also by single-crystal X-ray diffraction analysis.

Evaporating the solvent from the solution of commercial MgMeBr (3 M in Et_2O) at low pressure and drying the residue in vacuo for 1 h resulted in formation of a compound having the composition MgMeBr(Et_2O) (**3**). Dissolving **3** in thf provided the substitution of diethyl ether by thf. Evaporating the solvents in vacuo and drying the residue at 50 °C gave a white powder of the composition MgMeBr(thf) (**4**). Compounds **3** and **4** were isolated in quantitative yields (Scheme 3).

Equimolar amounts of MgMeBr and diglyme were reacted in thf solution. After stirring overnight the clear solution was cooled down to −80 °C to form a small quantity of crystals of the composition [$MgBr_2$(thf)$_4$]. After filtering off these crystals, the filtrate was concentrated in vacuo to form a white precipitate of

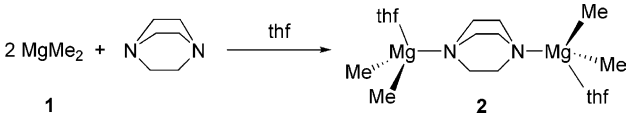

Scheme 2. Synthesis of [{$MgMe_2$(thf)}$_2$(μ-dabco)] (**2**).

MgMeBr(diglyme) (**5**) in 57% yield (Scheme 3). Reaction of MgMeBr with a threefold excess of triethylamine in diethyl ether followed by addition of *n*-hexane resulted in the formation of MgMeBr(NEt_3) (**6**) as a white highly air- and moisture-sensitive powder in nearly quantitative yield (Scheme 3). Addition of *N*,*N*,*N*′,*N*′-tetramethylethylenediamine (tmeda) to a diethyl ether solution of MgMeBr in an equimolar ratio proved to be strongly exothermic and resulted in precipitation of MgMeBr(tmeda) (**7**) also as a white powder in nearly quantitative yield. From a thf solution of **7** well shaped colorless crystals were crystallized at −40 °C; single-crystal X-ray diffraction analysis revealed the formation of a thf adduct [MgMeBr(thf)(tmeda)] (**8**). Drying these crystals in vacuo at room temperature for 1/2 h resulted in removing the thf molecule yielding again **7**. The overall composition for compounds **5**–**7** was deduced from microanalysis and NMR measurements.

Reaction of MgMeBr with an equimolar amount of *N*,*N*,*N*′,*N*″,*N*″-pentamethyldiethylenetriamine (pmdta) in tetrahydrofuran at room temperature revealed a clear solution. Cooling down to −40 °C provided a white powdery precipitate of [MgMeBr(pmdta)] (**9**) in nearly quantitative yield. On the other hand, the addition of pmdta to a diethyl ether solution of MgMeBr, instead of a thf solution, resulted in exothermic formation of a white powder having the composition MgMeBr(pmdta) · $MgBr_2$(pmdta) (**10**). After filtering off **10**, *n*-hexane was added to the filtrate to precipitate a small amount of white powder [{$MgMe_2$(pmdta)}$_7${MgMeBr(pmdta)}] (**11**). After filtration, concentrating the filtrate in vacuo again and cooling down to −40 °C gave rise to formation of big colorless needles of [$MgMe_2$(pmdta)] (**12**). Referring to the total magnesium content, precipitates **10**, **11**, and **12** were isolated in 24%, 2%, and 26% yields, respectively. The latter represents 52% of the theoretical yield of [$MgMe_2$(pmdta)] (Scheme 4).

The constitutions of precipitates **10** and **11** were deduced by microanalysis. Several parallel experiments afforded reproducible analytical results for both **10** and **11**. Furthermore, after filtering off compound **10**,

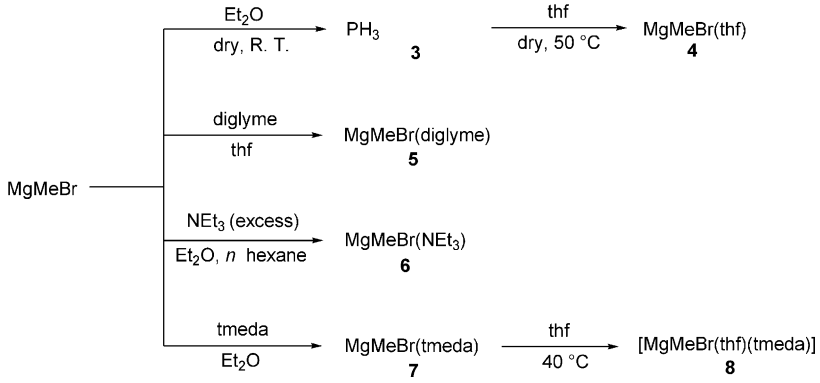

Scheme 3. Syntheses of MgMeBr(L) (L = Et_2O (**3**); thf (**4**); diglyme (**5**); NEt_3 (**6**); tmeda (**7**)) and [MgMeBr(thf)(tmeda)] (**8**).

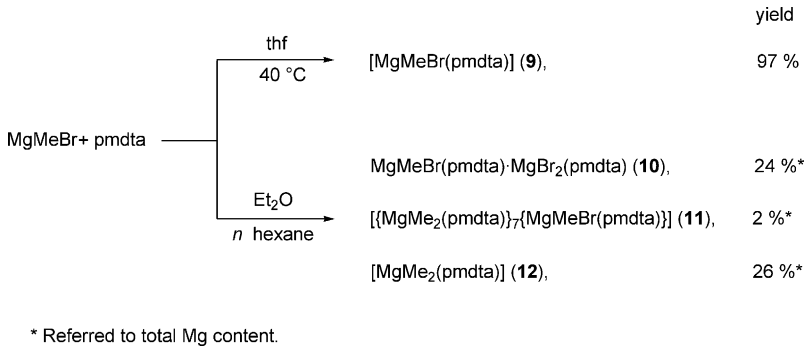

Scheme 4. Reactions of MgMeBr with pmdta in thf and in Et_2O.

the filtrate was cooled down to 5 °C to give colorless well-shaped crystals. The X-ray structure analysis of these crystals proved to be **11** · $2Et_2O$ in full agreement with the analytical results. The constitution of **12** was confirmed by NMR spectroscopy and single-crystal X-ray diffraction analysis. In most cases, **12** proved to be free of bromide. In few cases, some bromide traces were detected, thus **12** was recrystallized again from diethyl ether to provide completely bromide-free dimethylmagnesium pmdta complex.

The complex [$MgMe_2$(pmdta)] (**12**) was independently obtained by the reaction of $MgMe_2$ with pmdta in diethyl ether [19]. For this synthesis halide-free $MgMe_2$ was used as a starting material that is difficult to be synthesized in the "dioxane route" [3,6]. Moreover, the alternative transmetalation route using Mg and $HgMe_2$ should be excluded due to the extraordinarily high toxicity of the latter. Consequently, the route to **12**, as discussed in this paper, starting from easily accessible and less expensive MgMeBr and pmdta may be superior to the "classical" route from $MgMe_2$ and pmdta.

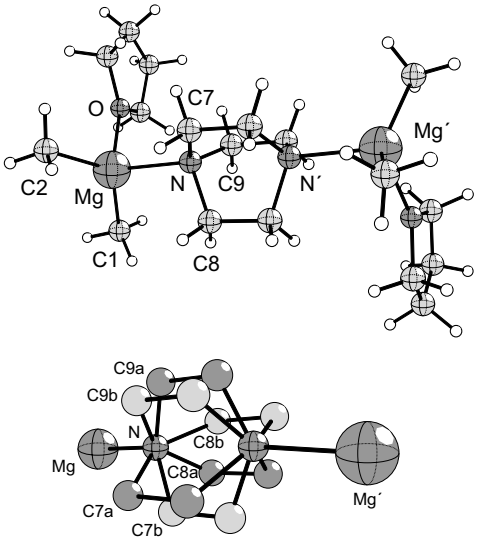

Fig. 1. Molecular structure of [{$MgMe_2$(thf)}$_2$(μ-dabco)] (**2**) (top) and disorder of the bridging dabco ligand (bottom). The two disordered positions are termed "a" and "b", atoms generated by a C_2 axis are marked with an asterisk. Selected bond lengths (Å) and angles (°): Mg–C1 2.127(4), Mg–C2 2.133(4), Mg–O 2.071(3), Mg–N 2.208(3); C1–Mg–C2 130.4(2), C1–Mg–O 105.2(2), C1–Mg–N 107.0(1), C2–Mg–O 106.4(2), C2–Mg–N 105.9(2), O–Mg–N 97.0(1).

2.2. Structures

Single crystals of compound **2** were found to be built up from binuclear molecules without unusual intermolecular contacts (shortest distance between non-hydrogen atoms is >3.5 Å). The molecular structure of [{$MgMe_2$(thf)}$_2$(μ-dabco)] (**2**) is shown in Fig. 1 with selected bond lengths and angles in the figure caption. The carbon atoms of the dabco ligand are disordered over two equally occupied positions amounting to an overall "rotation" of dabco around the N···N axis by about 45°. The binuclear complex exhibits crystallographically imposed C_2 symmetry. The magnesium atoms are tetrahedrally coordinated; the donor set is made up of one nitrogen, one oxygen, and two carbon atoms. The angle C1–Mg–C2 (130.4(2)°) is widened up at the expense of the O–Mg–N angle (97.0(1)°); all other angles are close to the tetrahedral standard (105.2(2)–107.0(1)°). Noteworthy, binuclear main-group metal complexes with bridging dabco ligands are rare. Apart from **2**, only two structures were reported in literature, namely [(MMe_3)$_2$(μ-dabco)] (M = Al, Ga) [20].

Crystals of [MgMeBr(thf)(tmeda)] (**8**) contain isolated molecules without unusual intermolecular contacts (shortest distance between non-hydrogen atoms is >3.7 Å). The molecular structure is shown in Fig. 2 with selected bond lengths and angles in the figure caption. The atoms of the thf ligand show a disorder over two equally occupied positions. Furthermore, the methyl and the bromo ligands are mutually disordered with an occupancy ratio of 0.64/0.36. Magnesium is coordinated in a trigonal bipyramide by carbon, bromine, oxygen, and two nitrogen atoms. As usual for trigonal-bipyramidal structures [21], the more electronegative ligands (thf, one N of tmeda) occupy the apical positions. The angle O–Mg–N2 is 166.5(5)°/161.9(6)°. Sum

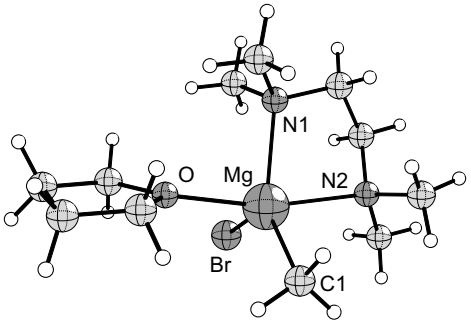

Fig. 2. Molecular structure of [MgMeBr(thf)(tmeda)] (**8**). Only one of disordered positions of Br/C1 and of thf atoms is shown (see Section 3.3). Selected bond lengths (Å) and angles (°) (for disordered positions both values are given separated by a slash; in the case of Br/C1 disorder values of the major occupied positions are given first): Mg–C1 2.25(1)/2.27(1), Mg–Br 2.485(1)/2.434(2), Mg–O 2.204(9)/2.22(1), Mg–N1 2.246(2), Mg–N2 2.334(3); N2–Mg–O 166.5(5)/161.9(6), C1–Mg–Br 126.0(4)/117.3(5), C1–Mg–N1 127.4(4)/111.9(5), N1–Mg–Br 106.57(7)/130.68(9).

of angles of the equatorial ligands (Br, C1, N1) is 360.0°/359.9°. A trigonal-bipyramidal geometry is an exception from the tendency to form a tetrahedral structure in normal Grignard reagents [15]. This may be due to the small size of the methyl group and the electronegativity of the bromo ligand. The only reported structure of a methylmagnesium bromide, namely [$MgMeBr(thf)_3$], shows also a disorder of the methyl and bromo ligands [16]. The Mg atom in this complex has a trigonal-bipyramidal coordination with two thf ligands in apical positions. Furthermore, the Mg–C bonds in complex **2** (C.N. 4; 2.127(4)/2.133(4) Å) are found to be shorter than those in complex **8** (C.N. 5; 2.25(1)/2.27(1) Å) being consistent with Gutmann's bond-length variation rules [22].

[$\{MgMe_2(pmdta)\}_7\{MgMeBr(pmdta)\}] \cdot 2Et_2O$ (**11** · $2Et_2O$) crystallizes in the monoclinic space group $P2_1/c$. The asymmetric unit contains two molecules of [$MgMe_2$(pmdta)] and [$MgMe_{1.75}Br_{0.25}$(pmdta)], respectively, and a half molecule of Et_2O, see Fig. 3. The mutual disorder between the methyl group and the bromine is described in the Section 3.3. Due to that, the numerical values given in the figure caption must not be overestimated.

The pmdta complexes [$MgMe_2$(pmdta)] (**12**) and [$MgBr_2$(pmdta)] (**13**) crystallize also in the monoclinic space group $P2_1/c$ with two crystallographically independent molecules in the asymmetric unit. The structures of these molecules are very similar, one of them is shown in Figs. 4 and 5 with selected bond lengths and angles in the figure captions. Viebrock and Weiss [19] prepared complex **12** from $MgMe_2$ and pmdta. They found essentially the same structure.

In both complexes the magnesium atoms are five-coordinated by three nitrogen and two carbon atoms in **12** and three nitrogen and two bromine atoms in **13**. The coordination polyhedra can be regarded as distorted square pyramides where the apical positions are occupied by a methyl ligand (C1) and a bromo ligand (Br1), respectively. The bond lengths of the apical ligands are significantly shorter than those of the corresponding basal ligands. Thus, the differences in the Mg–C and Mg–Br bond lengths amount to 0.036/0.016 and 0.061/0.089 Å, respectively. The apical ligands include angles with the basal ones in **12** between 99.4(2)–114.5(2)°/100.4(1)–115.8(1)° and in **13** between 99.4(2)–113.2(2)°/98.7(2)–110.3(2)°.

2.3. NMR spectroscopic measurements

The ^1H and ^{13}C resonances as well as the $^1J(C,H)$ coupling constants of methyl groups in the dimethylmagnesium and Grignard compounds described before in thf-d_8 solutions are given in Table 1. The coordination-induced shift differences $\Delta\delta_H$ and $\Delta\delta_C$ for hydrogen and carbon atoms of the ligands and the corresponding changes of $^1J(C,H)$ coupling constants are given in Table 2. As shown in the synthesis of MgMeBr(thf) (**4**), the diethyl ether molecule in MgMeBr(Et_2O) (**3**) is

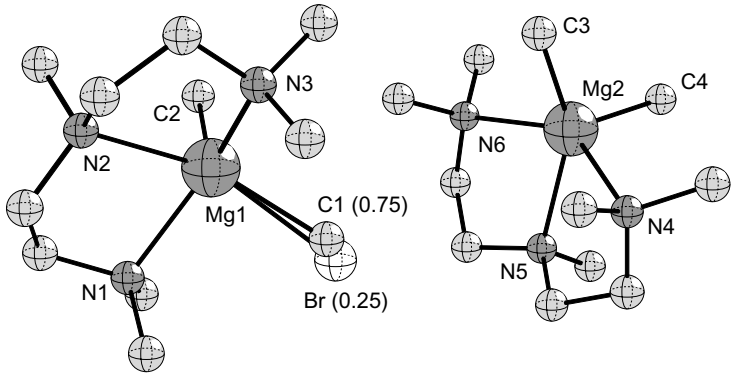

Fig. 3. Molecular structure of [$\{MgMe_2(pmdta)\}_7\{MgMeBr(pmdta)\}] \cdot 2Et_2O$ (**11** · $2Et_2O$). Hydrogen atoms and solvent molecules were omitted for clarity. In parentheses site occupancies of disordered atoms are given. Selected bond lengths (Å) and angles (°): Mg1–C1 2.238(6), Mg1–C2 2.161(2), Mg1–Br 2.580(2), Mg2–C3 2.256(2), Mg2–C4 2.247(2); C1–Mg1–C2 113.6(2), Br–Mg1–C2 111.7(1), C3–Mg2–C4 114.99(7).

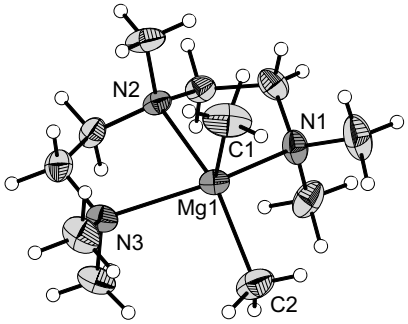

Fig. 4. Molecular structure of [$MgMe_2$(pmdta)] (**12**); displacement ellipsoids at 30% probability. One of the two crystallographically independent molecules is shown. Selected bond lengths (Å) and angles (°) (values for the two crystallographically independent molecules are given separated by a slash): Mg1–C1 2.162(3)/2.186(2), Mg1–C2 2.198(3)/2.202(2), Mg1–N1 2.347(2)/2.350(2), Mg1–N2 2.424(2)/2.391(2), Mg1–N3 2.357(2)/2.358(2); C1–Mg1–C2 114.5(2)/115.8(1), C1–Mg1–N1 106.7(2)/106.6(1), C1–Mg1–N2 99.4(2)/100.4(1), C1–Mg1–N3 108.5(2)/108.12(9), N1–Mg1–N3 136.07(8)/137.42(7).

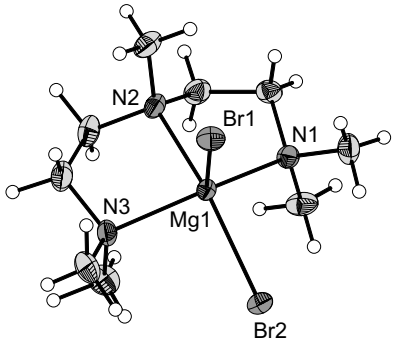

Fig. 5. Molecular structure of [$MgBr_2$(pmdta)] (**13**); displacement ellipsoids at 30% probability. One of the two crystallographically independent molecules is shown. Selected bond lengths (Å) and angles (°) (values for the two crystallographically independent molecules are given separated by a slash): Mg1–Br1 2.501(2)/2.482(2), Mg1–Br2 2.562(2)/2.571(2), Mg1–N1 2.205(6)/2.208(6), Mg1–N2 2.297(6)/2.310(6), Mg1–N3 2.224(5)/2.231(5); Br1–Mg1–Br2 103.02(7)/104.43(9), Br1–Mg1–N1 107.3(2)/110.3(2), Br1–Mg1–N2 99.4(2)/98.7(2), Br1–Mg1–N3 113.2(2)/108.1(2), N1–Mg1–N3 136.7(2)/137.9(2).

Table 1
The ^{1}H and ^{13}C resonances (δ in ppm) as well as ^1J(C,H) coupling constants (J in Hz) of methyl groups in methylmagnesium compounds **1**–**7**, **9**, **12** in thf-d_8 (concentration: 0.04 M, 27 °C)

Compound	δ_H	δ_C	^1J(C,H)
MgMeBr(Et_2O) (**3**)	−1.71	−16.4	106.3
MgMeBr(thf) (**4**)	−1.70	−16.3	106.6
MgMeBr(diglyme) (**5**)	−1.71	−16.0	106.4
MgMeBr(NEt_3) (**6**)	−1.71	−16.5	105.4
MgMeBr(tmeda) (**7**)	−1.67	−15.5	106.7
[MgMeBr(pmdta)] (**9**)	−1.67	−13.2	106.0
$MgMe_2$ (**1**)	−1.77	−16.9	105.7
[{$MgMe_2$(thf)}$_2$(μ-dabco)] (**2**)	−1.77	−16.8	105.6
[$MgMe_2$(pmdta)] (**12**)	−1.80	−14.1	104.6

cleaved off in thf (see Section 2.1). In accord with this observation, the NMR spectra of compounds **3** and **4** in thf are identical. The same holds for the triethylamine adduct **6**. The NMR data (Table 1) and the negligible coordination-induced shifts (Table 2) indicate that even NEt_3 may be substituted by a thf molecule in excess thf.

The resonances for methyl H and C atoms were high-field shifted and were found between −1.67 and −1.80 ppm (δ_H) and −13.2 and −16.9 ppm (δ_C). Such high-field shifts can be rationalized in terms of the polarity of Mg–CH_3 bonds [23]. The coupling constants ^1J(C,H) for the compounds shown in Table 1 were found to be within the range from 104.6 to 106.7 Hz revealing no significant dependence on the nature of coordinated ligands. These relatively low values reflect high *s*-electron densities in the Li–C bonds being consistent with the high electropositive character of Li and with Bent's rules [24].

Some general trends for proton and carbon chemical shifts could be deduced according to the nature of the ligand. Although the differences are small, the methyl protons of MgMeBr(L) resonate at slightly lower field for L = *N*-donor compared with L = *O*-donor, in contrast to dimethylmagnesium compounds where the opposite was found. On the other hand, the methyl-carbon resonances of complexes having chelating *N*-donor ligands are low-field shifted for both Grignard compounds and dimethylmagnesiums. Furthermore, methyl protons and carbon atoms in $MgMe_2$(L) compounds resonate at higher field compared with MgMeBr(L) (**1** versus **4** and **12** versus **9**).

The coordination-induced shifts $\Delta\delta_H$ and $\Delta\delta_C$ for H and C atoms of the ligands as well as the differences in ^1J(C,H) coupling constants are relatively small in all compounds under investigation (Table 2). In general, the same was found for these ligands in organolithium compounds [25]. Furthermore, the figures in Table 2 show that the strongest coordinating ligands (tmeda and pmdta) give rise to the highest induced shifts ($\Delta\delta$).

2.4. Schlenk equilibria in methylmagnesium bromide complexes

Methylmagnesium bromide complexes MgMeBr(L) (L = thf (**4**); diglyme (**5**); NEt_3 (**6**); tmeda (**7**); pmdta (**9**)) as well as the dimethylmagnesium compounds $MgMe_2$ (**1**) and [$MgMe_2$(pmdta)] (**12**) in thf-d_8 solutions at room temperature revealed sharp singlets for the methyl resonances in both ^{1}H and ^{13}C NMR spectra. Down to −80 °C, ^{1}H NMR spectrum of $MgMe_2$ (**1**) in thf-d_8 (0.04 mol/l) did show neither signal splitting nor broadening. This is fully consistent with the proposed monomeric constitution of $MgMe_2$ in thf solution at room temperature [26,27]. In contrast, $MgMe_2$ in diethyl ether is known to be associated via methyl bridges, thus showing at −80 °C two separated signals due to different

Table 2
The differences of ^{1}H and ^{13}C resonances ($\Delta\delta$ in ppm) and of $^{1}J(C,H)$ coupling constants (ΔJ in Hz) for coordinated ligands in methylmagnesium compounds **2**, **5**–**7**, **9**, **12** and corresponding free ligands in thf-d_8 at 27 °C

Compound	Ligand		$\Delta\delta_H$[a]	$\Delta\delta_C$ ($\Delta^1J(C,H)$)[a]
5	diglyme	CH_3	+0.05	+0.7 (+0.8)
		CH_2	+0.08	−0.4 (+1.7)
			+0.08	−0.4 (+1.2)
6	NEt_3	CH_3	−0.01	−0.1 (+0.2)
		CH_2	−0.01	0.0 (0.0)
2	dabco	CH_2	+0.02	−0.2 (0.0)
7	tmeda	CH_3	+0.17	+0.8 (+1.3)
		CH_2	+0.17	−1.2 (+2.9)
9	pmdta	CH_3N	+0.16	+1.9 (+3.7)
		$(CH_3)_2N$	+0.23	+0.6 (+6.7)
12	pmdta	CH_3N	+0.10	+0.3 (+2.6)
		$(CH_3)_2N$	+0.05	+1.5 (+3.8)

[a] $\Delta\delta = \delta_{coord.-lig.} - \delta_{free-lig.}$. $\Delta^1J(C,H) = {}^1J(C,H)_{coord.-lig.} - {}^1J(C,H)_{free-lig.}$.

methyl groups (terminal, bridging) [28]. But also in concentrated thf solutions of $MgMe_2$ (0.86 mol/l) signal splitting was observed at −76 °C. A major signal (−1.83 ppm) was attributed to $MgMe_2$ monomer and a smaller one (−1.70 ppm) to terminal sites in associated species [27]. Thus, our investigations gave evidence that $MgMe_2$ in thf remains to be monomeric even at −80 °C at a concentration of 0.04 mol/l.

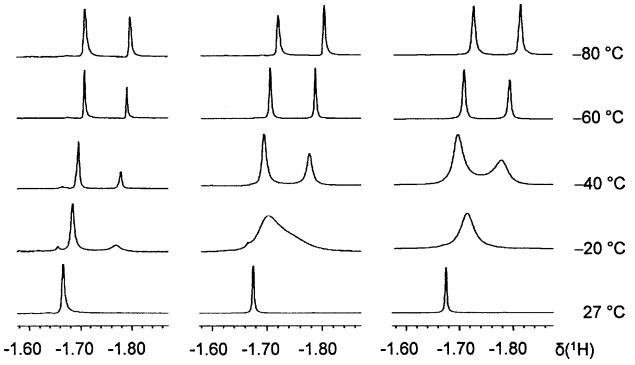

Fig. 6. Low-temperature ^{1}H NMR spectra of methyl protons for [MgMeBr(tmeda)] (**7**) in thf-d_8 (concentration dependence: 0.04 M, left; 0.12 M, middle; 0.25 M, right).

To gain an insight into the dynamic behavior of [MgMeBr(tmeda)] (**7**), the dependence of the methyl proton resonance on concentration as well as on temperature was investigated in thf-d_8 (Fig. 6). The spectra of **7** (concentrations 0.04–0.25 mol/l) revealed that the shift of the methyl protons is not markedly dependent on concentration. On the other hand, lowering the temperature of the solution resulted via line broadening into signal splitting; at −60 °C and below two sharp signals were observed.

The temperature dependence of ^{1}H NMR spectra for MgMeBr(thf) (**4**), MgMeBr(diglyme) (**5**), and MgMeBr(NEt_3) (**6**) in thf-d_8 solutions is shown in Fig. 7. As for **7**, at −60 °C and below two sharp singlet resonances were observed. Comparison with the ^{1}H NMR spectra of $MgMe_2$ (**1**) at temperatures down to −80 °C (see Fig. 7(d)) makes clear that the high-field shifted signal has to be assigned to dimethylmagnesium and the low-field shifted signal to methylmagnesium bromide. This order can be attributed to the deshielding caused by the electronegative bromo ligand, but the reverse order was also observed [6]. Inspection of the ratio of intensities showed that the lower the temperature the more the Schlenk equilibrium (Scheme 5, L = thf (**4**); diglyme (**5**); NEt_3 (**6**); tmeda (**7**)) is shifted to $MgMe_2$/$MgBr_2$. At −80 °C the equilibrium constant for the tmeda complex **7** can be roughly estimated to be approximately 0.25. On the other hand, in complexes **4**–**6** the dimethylmagnesium species are predominant; equilibrium constants were estimated to be about 5 to 10 at −80 °C. As discussed in Section 2.3, the triethylamine ligand in **6** may be substituted by thf in excess thf solvent.

In sharp contrast to the ^{1}H NMR spectra of **4**–**7**, an unexpected behavior of the pmdta complex [MgMeBr(pmdta)] (**9**) was observed (Fig. 8). Cooling

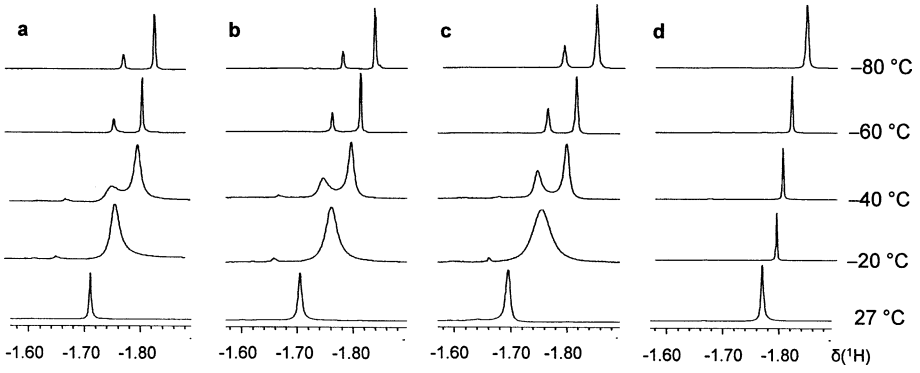

Fig. 7. Low-temperature ^{1}H NMR spectra of methyl protons for (a) MgMeBr(diglyme) (**5**), (b) MgMeBr(NEt_3) (**6**), (c) MgMeBr(thf) (**4**), and (d) $MgMe_2$ (**1**) in thf-d_8 (concentration: 0.04 M).

$$2\ [MgMeBr(L)] \rightleftharpoons [MgMe_2(L)] + [MgBr_2(L)]$$

Scheme 5. Schlenk equilibrium (L = thf, diglyme, NEt_3, tmeda, pmdta).

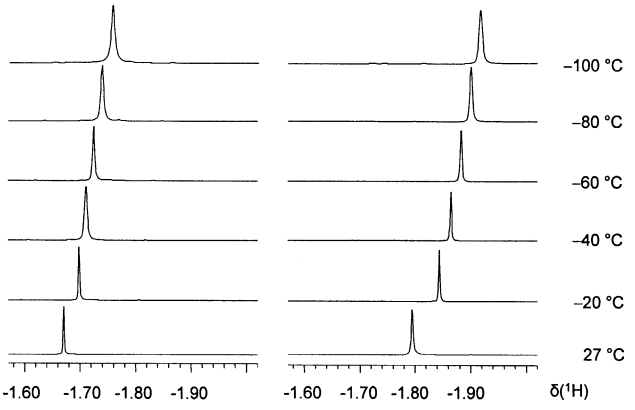

Fig. 8. Low-temperature ^{1}H NMR spectra of methyl protons for [MgMeBr(pmdta)] (**9**) (left) and [$MgMe_2$(pmdta)] (**12**) (right) in thf-d_8 (concentration: 0.04 M).

thf-d_8 solutions of **9** from room temperature down to −100 °C did not result in signal splitting but only in a slight high-field shift of the signal by about 0.1 ppm. Furthermore, as for [$MgMe_2$(pmdta)] (**12**) a slight line broadening was observed at −100 °C, which may be attributed to changes in solvent viscosity and to decreased quadrupolar relaxation time at lower temperatures [29].

[$MgBr_2$(pmdta)] (**13**) proved to be sparingly soluble in thf. But it was found to be dissolved immediately in the presence of one equivalent of [$MgMe_2$(pmdta)] (**12**), which indicates a complete reaction with **12** yielding quantitatively [MgMeBr(pmdta)] (**9**). In accordance with this observation, ^{1}H NMR investigations of the reaction mixture of **12** and **13** exhibited only one sharp signal for methyl protons of **9** at −1.68 ppm. To prove definetely that this is not a time averaged signal of **9/12** due to fast exchange reactions, more than one equivalent of [$MgMe_2$(pmdta)] (**12**) was reacted with **9**. Consequently, two signals were observed namely one at −1.68 ppm for [MgMeBr(pmdta)] (**9**) and another one at −1.81 ppm for the surplus [$MgMe_2$(pmdta)] (**12**). Thus, it was clearly shown that the position of the Schlenk equilibrium (Scheme 5, L = pmdta) in thf – even at room temperature – lies completely on the side of the Grignard reagent.

2.5. Quantum chemical calculations

To gain an insight into the position of the Schlenk equilibrium of methylmagnesium bromide in the presence of the pmdta ligand, quantum chemical calculations on the DFT level of theory were performed. The gas-phase optimized structures of [$MgMe_2$(pmdta)] (**12c**), [$MgBr_2$(pmdta)] (**13c**), and [MgMeBr(pmdta)] (**9c**) are shown in Fig. 9, selected bond lengths and angles are given in Table 3. Calculated structures [$MgMe_2$(pmdta)] (**12c**) and [$MgBr_2$(pmdta)] (**13c**) are consistent with the experimentally found structures **12** and **13**, respectively. Although there are some deviations in bond lenghts and angles, all important structural features are correctly reflected in the calculated structures. The two structures are best described as square pyramides with apical methyl and bromo ligand, respectively; there are severe distortions from trigonal bipyramides as shown by the angles N1–Mg–N3 137.0° for **12c** and 140.3° for **13c** (to be expected 180° in undistorted trigonal bipyramides). The Mg–L_{ap} bonds are considerably shorter than the Mg–L_{eq} bonds by 0.011 Å for L = Me and 0.064 Å for L = Br. The angles between these two ligands are 121.4° (**12c**) and 109.8° (**13c**). As for the experimentally found structures **12** and **13** the more electronegative bromo ligands in **13c** give rise to shorter Mg–N bonds than in **12c**. Furthermore, the Mg–N bonds of the two terminal N atoms of the pmdta ligands are shorter by 0.069 Å (**12c**) and 0.100 Å (**13c**) than that of the middle N atom.

An analogous structure was calculated for the Grignard type compound [MgMeBr(pmdta)] (**9c**), see Fig. 9 and Table 3. Experimental data for the structure of "pure" [MgMeBr(pmdta)] are not available. The only available compound is [{$MgMe_2$(pmdta)}$_7${MgMeBr(pmdta)}] · $2Et_2O$ (**11** · $2Et_2O$) (Fig. 3) where the structure of the [MgMeBr(pmdta)] molecule is close to the calculated structure **9c**. In complex **9c** the apical position of the distorted square pyramide is occupied by the more electronegative bromo ligand. Compared with the "symmetrically" substituted dimethyl- and dibromo compound **12c** and **13c**, respectively, the Mg–C bond is found to be shorter by 0.031 Å and the Mg–Br bond longer by 0.061 Å. The Mg–N bond lengths in the Grignard compound **9c** are shorter than those in the dimethyl compound **12c** but longer than those in the magnesium dibromide complex **13c**.

The energy for the disproportionation of the Grignard compound

$$2\ [\underset{\mathbf{9c}}{MgMeBr(pmdta)}] \rightleftharpoons [\underset{\mathbf{12c}}{MgMe_2(pmdta)}] + [\underset{\mathbf{13c}}{MgBr_2(pmdta)}]$$

was shown to be 4.86 kcal/mol at 0 K and 4.11 kcal/mol when the zero-point vibrational eneriges were taken into consideration. At 298 K the free reaction enthalpy was calculated to be $\Delta G_{gas} = 3.69$ kcal/mol [1] corresponding to an equilibrium constant $K_{gas} = 2.0 \times 10^{-3}$. In order

[1] Values calculated in the gas phase as well as in tetrahydrofuran and diethyl ether solution are marked by indices "gas", "thf", and "ether", respectively.

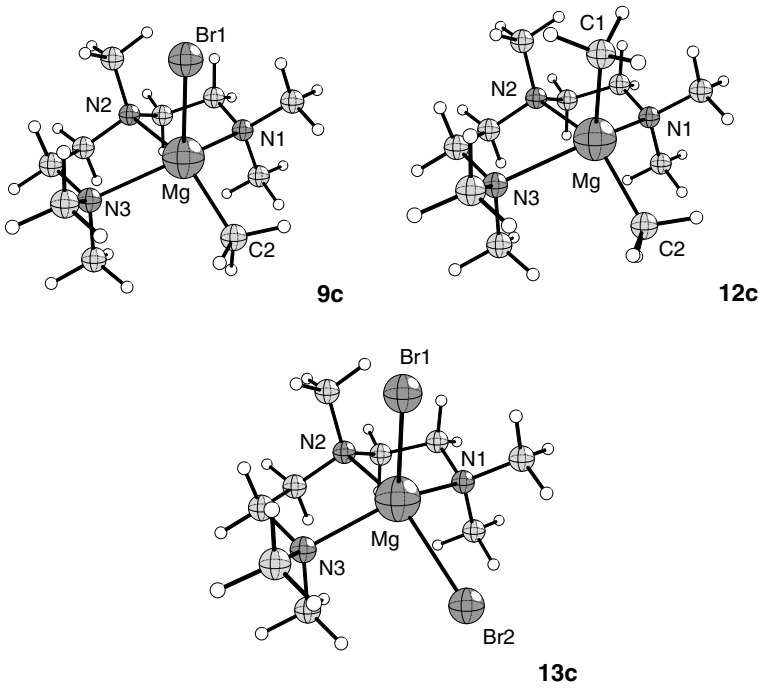

Fig. 9. Calculated structures of [MgMeBr(pmdta)] (**9c**), [$MgMe_2$(pmdta)] (**12c**), and [$MgBr_2$(pmdta)] (**13c**) along with their numbering schemes.

Table 3
Selected bond lengths (Å) and angles (°) for calculated complexes [$MgL_{ap}L_{eq}$(pmdta)] (L_{ap}/L_{eq} = Br/Me (**9c**); Me/Me (**12c**); Br/Br (**13c**))

	[MgMeBr(pmdta)] (**9c**) (L_{ap}/L_{eq} = Br1/C2H$_3$)	[$MgMe_2$(pmdta)] (**12c**) (L_{ap}/L_{eq} = C1H$_3$/C2H$_3$)	[$MgBr_2$(pmdta)] (**13c**) (L_{ap}/L_{eq} = Br1/Br2)
Mg–L_{ap}	2.617	2.165	2.556
Mg–L_{eq}	2.145	2.176	2.620
Mg–N1	2.354	2.426	2.255
Mg–N2	2.406	2.495	2.355
Mg–N3	2.354	2.426	2.255
N1–Mg–N3	144.5	137.0	140.3
L_{ap}–Mg–L_{eq}	115.6	121.4	109.8
L_{ap}–Mg–N1	102.8	106.1	107.8
L_{ap}–Mg–N2	95.8	97.5	96.7
L_{ap}–Mg–N3	102.8	106.2	107.8

to consider the solvent effects the Tomasi's polarized continuum model (PCM) was applied [30]. In tetrahydrofuran the free enthalpies of solvation at 298 K were calculated to be −3.27 kcal/mol for the Grignard compound **9c**, −6.24 kcal/mol for **13c** and −0.01 kcal/mol for the dimethylmagnesium compound **12c**. This means that the order of solvation is $MgBr_2$ > MgRBr > MgR_2, which meets the expectations. Due to ΔG_{solv}(**13c**) ≈ $2\Delta G_{solv}$(**9c**) and ΔG_{solv}(**12c**) ≈ 0 the influence of thf on the position of the Schlenk equilibrium is small: ΔG_{thf} was calculated at 298 K to be 3.98 kcal/mol corresponding to an equilibrium constant $K_{thf} = 1.2 \times 10^{-3}$. Thus, the quantum chemical calculations show clearly that in thf the Grignard compound [MgMeBr(pmdta)] (**9c**) does not disproportionate into **12c** and **13c** for thermodynamic reasons, which is fully consistent with the experimental findings.

The free enthalpies of solvation in diethyl ether were calculated to be −2.89 kcal/mol for [MgMeBr(pmdta)] (**9c**), −6.06 kcal/mol for [$MgBr_2$(pmdta)] (**13c**) and −0.01 kcal/mol for [$MgMe_2$(pmdta)] (**12c**). As expected (cf. the dielectric constants $\varepsilon/\varepsilon_0 = 4.3$, Et_2O; $\varepsilon/\varepsilon_0 = 7.6$, thf) they are very similar to those obtained for tetrahydrofuran. Thus, the influence of diethyl ether on the position of the Schlenk equilibrium is small ($\Delta G_{ether} = 3.40$ kcal/mol, $K_{ether} = 3.2 \times 10^{-3}$). Hence it follows that the synthesis of [$MgMe_2$(pmdta)] (**12**) directly from MgMeBr and pmdta in diethyl ether/*n*-hexane as described in Section 2.1 is based on the shift of the Schlenk equilibrium caused by the precipitation of sparingly soluble compounds. Thus, the dimer MgMeBr(pmdta) · $MgBr_2$(pmdta) (**10**) precipitates when pmdta is added to an etheral solution of MgMeBr. Furthermore, the desired complex [$MgMe_2$(pmdta)] (**12**) was found to

precipitate by adding *n*-hexane to the etheral reaction mixture.

In summary, some novel methylmagnesium compounds were synthesized via ligand-substitution reactions. Diethyl ether is only weakly coordinated to magnesium and was substituted by stronger basic monodentate (thf, NEt_3) as well as chelating bidentate (tmeda) and tridentate ligands (diglyme, pmdta). Noteworthy, the reaction of MgMeBr with pmdta proved to be strongly solvent dependent yielding in tetrahydrofuran [MgMeBr(pmdta)] (**9**) and in diethyl ether/*n*-hexane [$MgMe_2$(pmdta)] (**12**). Thus, a way was found to synthesize the dimethylmagnesium pmdta complex **12** from easily accessible reagents (MgMeBr/pmdta). Furthermore, studies of the Schlenk equilibrium of MgMeBr exhibited that it is shifted in the presence of the strongly coordinating and chelating pmdta ligand completely towards the Grignard reagent in thf and in diethyl ether solutions. The pronounced influence of the pmdta ligand on the position of the Schlenk equilibrium opens up new possibilities to study reactivities and mechanisms of Grignard reagents.

3. Experimental

3.1. General comments

All reactions and manipulations were carried out under purified argon using standard Schlenk techniques and a glove box from Fa. MB Braun, respectively. Thf-d_8, diglyme, triethylamine, *n*-hexane, tmeda, and pmdta were dried with $LiAlH_4$. Diethyl ether, 1,4-dioxane, and thf were distilled from sodium benzophenone ketyl. Dabco and MgMeBr (3 M in Et_2O) are commercially available from Merck and Fluka, respectively. ^1H and ^{13}C NMR spectra were recorded on Varian Unity 500, VXR 400, and Gemini 200 spectrometers. Protio impurities and ^{13}C resonances of thf-d_8 were used as internal standards. Microanalyses (C, H, N) were performed by the University of Halle microanalytical laboratory using a CHNS-932 (LECO) and Vario EL (elementar Analysensysteme) elemental analyzers, respectively. Bromine contents were determined by mercurimetric titration method [31].

For comparison ^1H NMR (400 MHz, 7.0 μl in 0.7 ml thf-d_8) and ^{13}C NMR (125 MHz, 40.0 μl in 0.7 ml thf-d_8) spectra of free *O*- and *N*-donor ligands were measured. *Diglyme*: ^1H NMR: δ 3.28 (s, 6H, CH_3), 3.44/3.53 (^2J(H,H) = −6.07 Hz/−4.10 Hz, ^3J(H,H) = 12.3/12.3 Hz, 4H/4H, CH_2) [32]. ^{13}C NMR: δ 58.4 (q, ^1J(C,H) = 140.1 Hz, *C*H$_3$), 71.4 (t, ^1J(C,H) = 140.1 Hz, *C*H$_2$OCH$_2$), 72.9 (t, ^1J(C,H) = 139.9 Hz, *C*H$_2$OCH$_3$). *NEt_3*: ^1H NMR: δ 0.97 (t, ^3J(H,H) = 7.06 Hz, 9H, CH_3), 2.44 (q, ^3J(H,H) = 7.12 Hz, 6H, CH_2). ^{13}C NMR: δ 12.7 (q, ^1J(C,H) = 124.8 Hz, *C*H$_3$), 47.3 (t, ^1J(C,H) = 131.0 Hz, *C*H$_2$). *Dabco*: ^1H NMR: δ 2.65 (s, CH_2). ^{13}C NMR: δ 48.7 (t, ^1J(C,H) = 138.2 Hz, *C*H$_2$). *Tmeda*: ^1H NMR: δ 2.15 (s, 12H, CH_3), 2.31 (s, 4H, CH_2). ^{13}C NMR: δ 46.2 (q, ^1J(C,H) = 131.8 Hz, *C*H$_3$), 58.9 (t, ^1J(C,H) = 131.5 Hz, *C*H$_2$). *Pmdta*: ^1H NMR: δ 2.15 (s, 3H, CH_3N), 2.20 (s, 12H, (CH_3)$_2$N), 2.31/2.42 (^2J(H,H) = −4.20/−3.54 Hz, ^3J(H,H) = 8.42/5.42 Hz, 4H/4H, CH_2) [32]. ^{13}C NMR: δ 42.3 (q, ^1J(C,H) = 132.1 Hz, *C*H$_3$N), 45.2 (q, ^1J(C,H) = 130.3 Hz, (*C*H$_3$)$_2$N), 56.4/57.9 (t/t, ^1J(C,H) = 131.7/131.2 Hz, 2 × *C*H$_2$).

3.2. Syntheses

3.2.1. $MgMe_2$ (*1*)

To a solution of MgMeBr (83.7 mmol) in diethyl ether (60 ml), 1,4-dioxane (8.26 g, 93.7 mmol) was added dropwise at 0 °C. Immediately, a white precipitate was formed and then the solution was stirred for 4 d before filtration. The filtrate was cooled down to −40 °C to provide after 1 d colorless rectangular-shaped crystals, which were filtered off and dried in vacuo for 1/2 h to give **1**. Yield: 0.65 g (29%). Anal. Calc. for C_2H_6Mg (54.37): C, 44.18; H, 11.12; Br, 0.00. Found: C, 42.77; H, 10.89; Br, <0.2%. ^1H NMR (500 MHz, thf-d_8): δ −1.81 (s, CH_3Mg). ^{13}C NMR (125 MHz, thf-d_8): δ −16.9 (q, ^1J(C,H) = 105.7 Hz, *C*H$_3$Mg). ^1H NMR (500 MHz, thf-d_8), temperature dependence of δ(CH_3); concentration 0.04 mol/l: −1.772 (27 °C), −1.791 (−20 °C), −1.803 (−40 °C), −1.818 (−60 °C), −1.844 (−80 °C).

3.2.2. [{$MgMe_2$(thf)}$_2$(μ-dabco)] (*2*)

To a solution of $MgMe_2$ (**1**) (0.27 g, 5.0 mmol) in thf (10 ml), dabco (0.30 g, 2.7 mmol) was added and stirred for 1 h to give a clear yellowish solution. This solution was cooled down to −40 °C for 3 d to form colorless sticky crystals of **2**, whose structure was determined by single-crystal X-ray diffraction. When these crystals were filtered off and dried in vacuo for 1/2 h, a white precipitate was formed. Yield: 0.77 g (84%). Anal. Calc. for $C_{18}H_{40}Mg_2O_2N_2$ (365.13): C, 59.21; H, 11.04; N, 7.67. Found: C, 58.56; H, 11.20; N, 7.85%. ^1H NMR (400 MHz, thf-d_8): δ −1.77 (s, 12H, CH_3Mg), 1.78 (m, 8H, CH_2CH$_2$O), 2.67 (s, 12H, CH_2N), 3.62 (m, 8H, CH$_2$O). ^{13}C NMR (125 MHz, thf-d_8): δ −16.8 (q, ^1J(C,H) = 105.6 Hz, *C*H$_3$Mg), 26.4 (t, ^1J(C,H) = 131.6 Hz, *C*H$_2$CH$_2$O), 48.5 (t, ^1J(C,H) = 138.2 Hz, *C*H$_2$N), 68.2 (t, ^1J(C,H) = 143.5 Hz, *C*H$_2$O).

3.2.3. MgMeBr(L), L = (Et_2O, (*3*); thf, (*4*))

From a solution of MgMeBr (15.5 mmol) in diethyl ether (5 ml) the solvent was removed and the residue was dried in vacuo at RT for 1 h to give a white powder of **3**. Yield: 2.9 g (97%). ^1H NMR (200 MHz, thf-d_8): δ −1.71 (s, 3H, CH_3Mg), 1.10 (t, ^3J(H,H) = 6.96 Hz, 6H,

CH_3CH_2O), 3.38 (q, ^3J(H,H) = 7.00 Hz, 4H, CH_3CH_2O). ^{13}C NMR (125 MHz, thf-d_8): δ −16.4 (q, ^1J(C,H) = 106.3 Hz, CH_3Mg), 15.7 (q, ^1J(C,H) = 125.6 Hz, C H_3CH_2O), 66.3 (t, ^1J(C,H) = 139.1 Hz, CH_3CH_2O).

A sample of **3** (2.50 g, 12.9 mmol) was dissolved in thf (40 ml) and stirred for 1/2 h. The solvents were evaporated in vacuo at RT. Then the residue was dried in vacuo at 50 °C for 1 h to give a white powder **4**. Yield: 2.4 g (97%). Anal. Calc. for $C_5H_{11}BrMgO$ (191.35): C, 31.38; H, 5.79; Br, 41.76. Found: C, 31.78; H, 5.37; Br, 39.67%. ^{1}H NMR (200 MHz, thf-d_8): δ −1.75 (s, CH_3Mg). ^{13}C NMR (125 MHz, thf-d_8): δ −16.3 (q, ^1J(C,H) = 106.6 Hz, CH_3Mg). ^{1}H NMR (500 MHz, thf-d_8), temperature dependence of $\delta(CH_3)$; concentration 0.04 mol/l: −1.695 (27 °C), −1.769 (−20 °C), −1.748/−1.800 (−40 °C), −1.767/−1.817 (−60 °C), −1.786/−1.844 (−80 °C).

3.2.4. MgMeBr(diglyme) (5)

A solution of MgMeBr (18.6 mmol) in diethyl ether (6 ml) was concentrated in vacuo up to ca. 1 ml, and subsequently thf (50 ml) was added. Diglyme (2.63 g, 19.6 mmol) was added dropwise and then the reaction mixture was stirred overnight at RT. The clear solution was cooled down to −80 °C for 1 d to form a small quantity of colorless needles of [$MgBr_2(thf)_4$], which were filtered off and dried in vacuo for 1/2 h (Anal. Calc. for $C_{16}H_{32}Br_2MgO_4$ (472.54): C, 40.67; H, 6.83. Found: C, 40.71; H, 6.53%. ^{1}H and ^{13}C NMR: no other than thf signals). The filtrate was concentrated up to ca. 15 ml to precipitate a white powder of **5**, which was filtered off and dried in vacuo for 1/2 h. Yield: 2.7 g (57%). Anal. Calc. for $C_7H_{17}BrMgO_3$ (253.42): C, 33.18; H, 6.76; Br, 31.53. Found: C, 33.35; H, 6.70; Br, 31.48%. ^{1}H NMR (400 MHz, thf-d_8): δ −1.73 (s, 3H, CH_3Mg), 3.33 (s, 6H, CH_3O), 3.52/3.61 (^2J(H,H) = −6.07/−4.14 Hz, ^3J(H,H) = 11.03/11.26 Hz, 4H/4H, CH_2O) [32]. ^{13}C NMR (125 MHz, thf-d_8): δ −16.0 (q, ^1J(C,H) = 106.4 Hz, C H_3Mg), 59.1 (q, ^1J(C,H) = 140.9 Hz, CH_3O), 71.0 (t, ^1J(C,H) = 141.8 Hz, CH_2OCH_2), 72.5 (t, ^1J(C,H) = 141.1 Hz, CH_2OCH_3). ^{1}H NMR (500 MHz, thf-d_8), temperature dependence of $\delta(CH_3)$; concentration 0.04 mol/l: −1.712 (27 °C), −1.767 (−20 °C), −1.754/−1.800 (−40 °C), −1.766/−1.817 (−60 °C), −1.784/−1.839 (−80 °C).

3.2.5. MgMeBr(NEt_3) (6)

To a solution of MgMeBr (19.2 mmol) in diethyl ether (30 ml), NEt_3 (5.81 g, 57.4 mmol) was added dropwise with stirring. After 4 h the solution was concentrated in vacuo up to about 10 ml. Then *n*-hexane (30 ml) was added to precipitate a white powder of **6**, which was filtered off, washed with *n*-hexane (2 × 5 ml), and dried in vacuo for 1/2 h. Yield: 4.1 g (97%). Anal. Calc. for $C_7H_{18}BrMgN$ (220.43): C, 38.14; H, 8.23; Br, 36.25; N, 6.35. Found: C, 37.33; H, 8.28; Br, 36.36; N, 6.08%. ^{1}H NMR (400 MHz, thf-d_8): δ −1.72 (s, 3H, CH_3Mg), 0.96 (t, ^3J(H,H) = 7.11 Hz, 9H, CH_3CH_2N), 2.43 (q, ^3J(H,H) = 7.11 Hz, 6H, CH_2N). ^{13}C NMR (125 MHz, thf-d_8): δ −16.5 (q, ^1J(C,H) = 105.4 Hz, CH_3Mg), 12.6 (q, ^1J(C,H) = 125.0 Hz, CH_3CH_2N), 47.3 (t, ^1J(C,H) = 131.0 Hz, CH_2N). ^{1}H NMR (500 MHz, thf-d_8), temperature dependence of $\delta(CH_3)$; concentration 0.04 mol/l: −1.706 (27 °C), −1.765 (−20 °C), −1.750/−1.800 (−40 °C), −1.767/−1.817 (−60 °C), −1.785/−1.842 (−80 °C).

3.2.6. MgMeBr(tmeda) (7) and [MgMeBr(thf)(tmeda)] (8)

To a solution of MgMeBr (16.0 mmol) in diethyl ether (25 ml), a solution of tmeda (2.08 g, 17.9 mmol) in diethyl ether (3 ml) was added dropwise to give a white precipitate of **7** in an exothermic process. The precipitate was filtered off, washed with diethyl ether (2 × 4 ml), and dried in vacuo for 1/2 h. Yield: 3.7 g (98%). Anal. Calc. for $C_7H_{19}BrMgN_2$ (235.45): C, 35.71; H, 8.13; Br, 33.94; N, 11.90. Found: C, 35.13; H, 7.97; Br, 35.54; N, 11.61%. ^{1}H NMR (400 MHz, thf-d_8): δ −1.67 (s, 3H, CH_3Mg), 2.32 (s, 12H, CH_3N), 2.48 (s, 4H, CH_2N). ^{13}C NMR (125 MHz, thf-d_8): δ −15.5 (q, ^1J(C,H) = 106.7 Hz, CH_3Mg), 47.0 (q, ^1J(C,H) = 133.1 Hz, CH_3N), 57.7 (t, ^1J(C,H) = 134.4 Hz, CH_2N). ^{1}H NMR (500 MHz, thf-d_8), temperature dependence of $\delta(CH_3)$: concentration 0.04 mol/l: −1.668 (27 °C), −1.690/−1.778 (−20 °C), −1.702/−1.788 (−40 °C), −1.714/−1.800 (−60 °C), −1.724/−1.812 (−80 °C); concentration 0.12 mol/l: −1.677 (27 °C), −1.705 (−20 °C), −1.698/−1.787 (−40 °C), −1.710/−1.799 (−60 °C), −1.724/−1.814 (−80 °C); concentration 0.25 mol/l: −1.678 (27 °C), −1.717 (−20 °C), −1.701/−1.786 (−40 °C), −1.712/−1.802 (−60 °C), −1.727/−1.818 (−80 °C).

A solution of **7** (50 mg) in thf (1 ml) was cooled down to −40 °C. After 3 d colorless crystals of **8** were formed, which their structure was measured by single-crystal X-ray diffraction analysis. When these crystals were isolated and dried in vacuo for 1/2 h they lost the thf (^{1}H and ^{13}C NMR spectra are as described above for **7**).

3.2.7. [MgMeBr(pmdta)] (9)

A solution of MgMeBr (15.8 mmol) in diethyl ether (5 ml) was concentrated in vacuo up to about 1 ml. Then thf (50 ml) was added. After dropwise addition of pmdta (2.91 g, 16.8 mmol), the solution was stirred overnight at RT. When the clear solution was cooled down to −40 °C for 1 d, compound **9** was precipitated as a white powder, which was filtered off and dried in vacuo for 1/2 h. Yield: 4.5 g (97%). Anal. Calc. for $C_{10}H_{26}BrMgN_3$ (292.54): C, 41.06; H, 8.96; Br, 27.31; N, 14.36. Found: C, 41.01; H, 9.00; Br, 25.87; N, 14.23%. ^{1}H NMR (500 MHz, thf-d_8): δ −1.68 (s, 3H, CH_3Mg), 2.31 (s, 3H, CH_3N), 2.43 (s, 12H, $(CH_3)_2N$), 2.54/2.70 (br/br, 4H/4H, 2 × CH_2N).

^{13}C NMR (125 MHz, thf-d_8): δ −13.2 (q, ^1J(C,H) = 106.0 Hz, CH_3Mg), 44.2 (q, ^1J(C,H) = 135.8 Hz, CH_3N), 45.8 (q, ^1J(C,H) = 137.0 Hz, $(CH_3)_2$N), 57.4/57.6 (t/t, ^1J(C,H) = 134.0/133.7 Hz, 2 × CH_2N). ^{1}H NMR (500 MHz, thf-d_8), temperature dependence δ(CH_3); concentration 0.04 mol/l: −1.672 (27 °C), −1.702 (−20 °C), −1.712 (−40 °C), −1.726 (−60 °C), −1.741 (−80 °C), −1.757 (−100 °C).

3.2.8. [$MgMe_2$(pmdta)] (**12**)

To a solution of MgMeBr (75.6 mmol) in diethyl ether (90 ml), a solution of pmdta (14.97 g, 86.4 mmol) in diethyl ether (20 ml) was added dropwise. Immediately, a white precipitate of MgMeBr(pmdta) · $MgBr_2$(pmdta) (**10**) was formed in an exothermic process. After stirring for 5 h, the precipitate was filtered off and dried in vacuo to give **10**. The filtrate was concentrated in vacuo up to about 30–40 ml to form a small amount of a precipitate, which was filtered off. *n*-Hexane (60 ml) was added to the filtrate to form a white precipitate [{$MgMe_2$(pmdta)}$_7${MgMeBr(pmdta)}] (**11**), which was filtered off. The resulted filtrate was concentrated in vacuo up to 50 ml and cooled down to −40 °C. After 1 d colorless needle-like crystals of **12** were formed, which were filtered off, washed with cold *n*-hexane, and dried in vacuo. Noteworthy, when the filtrate, after isolating **10** and before adding *n*-hexane, was cooled down to 5 °C for 3 d, colorless crystals of **11** · 2Et_2O were obtained, whose structure was confirmed by single-crystal X-ray diffraction analysis.

MgMeBr(pmdta) · $MgBr_2$(pmdta) (**10**): Yield: 6.0 g (24%, referred to total Mg content). Anal. Calc. for $C_{19}H_{49}Br_3Mg_2N_6$ (649.95): C, 35.11; H, 7.60; Br, 36.88; N, 12.93. Found: C, 35.39; H, 7.65; Br, 36.81; N, 12.83%.

[{$MgMe_2$(pmdta)}$_7${MgMeBr(pmdta)}] (**11**): Yield: 0.35 g (2%, referred to total Mg content). Anal. Calc. for $C_{87}H_{229}BrMg_8N_{24}$ (1886.25): C, 55.40; H, 12.24; Br, 4.24; N, 17.82. Found: C, 55.40; H, 12.31; Br, 4.20; N, 18.04%. ^{1}H NMR (400 MHz, thf-d_8): δ −1.80 (s, 42H, $(CH_3)_2$Mg), −1.68 (s, ca. 3H, CH_3MgBr), 2.27 (s, 24H, CH_3N), 2.32 (s, 96H, $(CH_3)_2$N), 2.45/2.60 (s/s, 32H/32H, CH_2N). ^{13}C NMR (100 MHz, thf-d_8): δ −14.5 (s, $(CH_3)_2$Mg), −13.6 (br, CH_3MgBr), 43.5 (s, CH_3N), 46.4 (s, $(CH_3)_2$N), 57.4/57.7 (s/s, CH_2N).

[$MgMe_2$(pmdta)] (**12**): Yield: 4.52 g (26%, referred to total Mg content). ^{1}H NMR (400 MHz, thf-d_8): δ −1.81 (s, 6H, CH_3Mg), 2.25 (s, 15H, CH_3N), 2.46/2.57 (m/m, 4H/4H, 2 × CH_2N). ^{13}C NMR (125 MHz, thf-d_8): δ −14.1 (q, ^1J(C,H) = 104.6 Hz, CH_3Mg), 42.6 (q, ^1J(C,H) = 134.7 Hz, CH_3N), 46.7 (q, ^1J(C,H) = 134.1 Hz, $(CH_3)_2$N), 57.6 (t, ^1J(C,H) = 135.0 Hz, CH_2N). ^{1}H NMR (500 MHz, thf-d_8), temperature dependence of δ(CH_3); concentration 0.04 mol/l: −1.795 (27 °C), −1.846 (−20 °C), −1.867 (−40 °C), −1.884 (−60 °C), −1.901 (−80 °C), −1.917 (−100 °C).

3.2.9. [$MgBr_2$(pmdta)] (**13**)

1,2-Dibromoethane (0.87 g, 4.64 mmol) in thf (36 ml) was added dropwise to magnesium metal (0.21 g, 8.64 mmol) in thf (10 ml) and stirred overnight. The residual metal was filtered off and to the clear filtrate pmdta (0.83 g, 4.79 mmol) was added dropwise to form immediately a white precipitate of **13**. This precipitate was filtered off, washed with boiling thf (5 times), and dried in vacuo for 8 h. Yield: 1.5 g (90%). Anal. Calc. for $C_9H_{23}Br_2MgN_3$ (357.41): C, 30.24; H, 6.49; Br, 44.71; N, 11.76. Found: C, 29.90; H, 6.42; Br, 44.28; N, 11.46%.

3.3. Crystallographic studies

Single crystals which were suitable for X-ray diffraction measurements were obtained as follows: **2** (colorless sticks, 0.7 × 0.4 × 0.3 mm) grown from thf solution at −40 °C; **8** (colorless blocks, 0.4 × 0.3 × 0.2 mm) grown from thf solution at −40 °C; **11** · 2Et_2O (colorless blocks, 0.2 × 0.3 × 0.4 mm) grown from Et_2O solution at 5 °C; **12** (colorless needles) from Et_2O/*n*-hexane solution at −40 °C; **13** (colorless needles) grown from thf solution at room temperature. Intensity data were collected on a Bruker Smart CCD (**2**, **8**, **11** · 2Et_2O) and STOE imaging plate diffraction system (**12**, **13**), respectively, with Mo-Kα radiation (0.71073 Å, graphite monochromator). A summary of crystallographic data, data collection parameters, and refinement parameters is given in Table 4. Absorption corrections were performed for **2** (SADABS, multi-scan; T_{min}/T_{max} = 0.36/1.00), **8** (SADABS, multi-scan; T_{min}/T_{max} = 0.88/1.00), **11** · 2Et_2O (SADABS, multi-scan; T_{min}/T_{max} = 0.93/1.00), and **13** (numerically; T_{min}/T_{max} = 0.25/0.65). The structures were solved by direct methods with SHELXS-97 and refined using full-matrix least-squares routines against F^2 with SHELXL-97 [33]. Non-hydrogen atoms were refined with anisotropic (except for C1/C1′ in **8**) and hydrogen atoms with isotropic displacement parameters. H atoms were added to the model in their calculated positions (riding model) (**2**, **8**, **11** · 2Et_2O) and found in the electron density maps (**12**, **13**), respectively. In **2** the carbon atoms of dabco ligand are disordered over two positions that are equally occupied. In **8** bromo and methyl ligands are disordered over two positions with site occupancies 0.64/0.36, whereas atoms of thf ligand are disordered over two positions with equally occupied positions. In crystals of **11** · 2Et_2O the asymmetric unit contains two molecules of [$MgMe_2$(pmdta)] and [$MgMe_{1.75}Br_{0.25}$(pmdta)], respectively, and a half molecule of Et_2O. The site occupancies for C1H3/Br were refined to be 0.72/0.28 and have been fixed at the end of the refinement to 0.75/0.25. Furthermore, a disordered diethyl ether molecule has been found with site occupancies refined to 0.30/0.20. Thus the diethyl ether molecule occupies only half of the "holes" in the crystal.

Table 4
Crystal data and structure refinement for **2**, **8**, **11** · $2Et_2O$, **12** and **13**

	2	**8**	**11** · $2Et_2O$	**12**	**13**
Empirical formula	$C_{18}H_{40}Mg_2N_2O_2$	$C_{11}H_{27}BrMgN_2O$	$C_{23.75}H_{62.25}Br_{0.25}Mg_2N_6O_{0.50}$	$C_{11}H_{29}MgN_3$	$C_9H_{23}Br_2MgN_3$
Formula weight	365.14	307.57	508.64	227.68	357.43
T (K)	183(2)	203(2)	198(2)	220(2)	220(2)
Crystal system	Monoclinic	Orthorhombic	Monoclinic	Monoclinic	Monoclinic
Space group	$C2/c$	$Pbca$	$P2_1/c$	$P2_1/c$	$P2_1/c$
a (Å)	23.799(3)	11.1743(10)	17.1465(6)	8.588(2)	8.486(1)
b (Å)	8.0779(8)	12.1611(11)	8.3947(3)	29.784(6)	30.054(4)
c (Å)	11.9984(12)	22.832(2)	23.9605(9)	12.511(3)	12.357(2)
β (°)	96.853(2)		102.421(1)	101.40(2)	100.72(2)
V (Å^3)	2290.2(4)	3102.7(5)	3368.1(2)	3137(1)	3096.5(8)
Z	4	8	4	8	8
ρ_{calc} (g/cm^3)	1.059	1.317	1.003	0.964	1.533
μ(Mo-Kα) (mm^{-1})	0.116	2.676	0.389	0.094	5.255
F(000)	808	1296	1134	1024	1440
Scan range (°)	1.72–26.43	1.78–26.41	1.74–26.02	2.15–26.07	2.16–26.04
Number of reflections collected	10020	36260	39488	22118	18857
Number of independent reflections (R_{int})	2516 (0.0710)	3167 (0.0464)	6632 (0.0347)	5778 (0.0851)	6025 (0.0781)
Data/restraints/parameters	2347/38/139	3167/38/205	6632/151/358	5778/0/503	6025/0/456
Goodness-of-fit on F^2	1.029	1.128	1.040	0.990	1.065
R_1, wR_1 [$I > 2\sigma(I)$]	0.0679, 0.1704	0.0400, 0.1052	0.0521, 0.1452	0.0471, 0.1090	0.0502, 0.1272
R_2, wR_2 (all data)	0.1131, 0.1945	0.0513, 0.1100	0.0665, 0.1566	0.0878, 0.1246	0.0864, 0.1516
Largest difference in peak/hole (e/Å^3)	0.344/−0.326	0.392/−0.421	0.512/−0.257	0.191/−0.189	0.774/−1.120

3.4. Computational details

All DFT calculations were carried out by the GAUSSIAN-98 program package [34] using the hybrid functional B3LYP [35]. All systems have been fully optimized without any symmetry restrictions using the SDD basis set of atomic orbitals as implemented in the GAUSSIAN-98 program. The resulting geometries were characterized as equilibrium structures by the analysis of the force constants of normal vibrations. To model the solvent influence (thf, Et_2O) on the energetics single-point PCM calculations on the gas-phase optimized structures were performed using the implementation in the GAUSSIAN-98 program package.

Acknowledgements

Financial support by the Deutsche Forschungsgemeinschaft and the Fonds der Chemischen Industrie is gratefully acknowledged. Furthermore, we thank Merck (Darmstadt) for gifts of chemicals.

Appendix A. Supplementary material

Crystallographic data (excluding structure factors) have been deposited at the Cambridge Crystallographic Data Center as supplementary publications Nos. CCDC-253752 (**2**), CCDC-253753 (**8**), CCDC-253754 (**11** · $2Et_2O$), CCDC-253755 (**12**), and CCDC-253756 (**13**). Copies of the data can be obtained free of charge on application to CCDC, 12 Union Road, Cambridge, CB2 1EZ, UK [fax: (internat.) +44 1223 336 033; e-mail: deposit@ccdc.cam.ac.uk]. Tables of Cartesian coordinates of atom positions calculated for equilibrium structures **9c**, **12c**, and **13c**. Supplementary data associated with this article can be found, in the online version at doi:10.1016/j.jorganchem.2004.10.058.

References

[1] A. Inoue, K. Oshima, in: H. Yamamoto, K. Oshima (Eds.), Main Group Metals in Organic Synthesis, Wiley–VCH, Weinheim, 2004, pp. 51–154.
[2] H.G. Richey, Jr. (Ed.), Grignard Reagents: New Developments, Wiley, Chichester, 2000.
[3] B.J. Wakefield, Organomagnesium Methods in Organic Synthesis, Academic Press, London, 1995.
[4] K.C. Cannon, G.R. Krow, in: G.S. Silverman, P.E. Rakita (Eds.), Handbook of Grignard Reagents, Marcel Dekker, New York, 1996, pp. 271–289.
[5] W. Schlenk, W. Schlenk Jr., Chem. Ber. 62 (1929) 920–924.
[6] W.E. Lindsell, in: G. Wilkinson, F.G.A. Stone, E.W. Abel (Eds.), Comprehensive Organometallic Chemistry, vol. 1, Pregamon Press, Oxford, 1982, pp. 155–252.
[7] W.E. Lindsell, in: E.W. Abel, F.G.A. Stone, G. Wilkinson (Eds.), Comprehensive Organometallic Chemistry II, vol. 1, Pregamon Press/Elsevier, Oxford, 1995, pp. 57–127.
[8] J. Axten, J. Troy, P. Jiang, M. Trachtman, C.W. Bock, Struct. Chem. 5 (1994) 99–108.
[9] A.W. Ehlers, G.P.M. van Klink, M.J. van Eis, F. Bickelhaupt, P.H.J. Niederkoorn, K. Lammertsma, J. Mol. Model. 6 (2000) 186–194.
[10] J. Tammiku, P. Burk, A. Tuulmets, J. Phys. Chem. A 105 (2001) 8554–8561.

[11] J. Tammiku-Taul, P. Burk, A. Tuulmets, J. Phys. Chem. A 108 (2004) 133–139.
[12] W. Schlenk, Jr., Chem. Ber. 64 (1931) 736–739.
[13] F. Bickelhaupt, in: H.G. Richey, Jr. (Ed.), Grignard Reagents: New Developments, Wiley, Chichester, 2000, pp. 299–328.
[14] H.L. Uhm, in: G.S. Silverman, P.E. Rakita (Eds.), Handbook of Grignard Reagents, Marcel Dekker, New York, 1996, pp. 117–144.
[15] P.R. Markies, O.S. Akkerman, F. Bickelhaupt, W.J.J. Smeets, A.L. Spek, Adv. Organomet. Chem. 32 (1991) 147–226.
[16] M. Vallino, J. Organomet. Chem. 20 (1969) 1–10.
[17] S. Sakamoto, T. Imamoto, K. Yamaguchi, Org. Lett. 3 (2001) 1793–1795.
[18] M. Veith, A. Spaniol, J. Pöhlmann, F. Gross, V. Huch, Chem. Ber. 126 (1993) 2625–2635.
[19] H. Viebrock, E. Weiss, J. Organomet. Chem. 464 (1994) 121–126.
[20] A.M. Bradford, D.C. Bradley, M.B. Hursthouse, M. Motevalli, Organometallics 11 (1992) 111–115.
[21] J.E. Huheey, E.A. Keiter, R.L. Keiter, Inorganic Chemistry, Principles of Structure and Reactivity, fourth ed., Harper–Collins, New York, 1993.
[22] V. Gutmann, The Donor–Acceptor Approach to Molecular Interactions, Plenum Press, New York, 1978, pp. 1–16.
[23] G. Fraenkel, D.G. Adams, J. Williams, Tetrahedron Lett. (1963) 767–773.
[24] H.A. Bent, Chem. Rev. 61 (1961) 275–311.
[25] S. Schade, G. Boche, J. Organomet. Chem. 550 (1998) 359–379.
[26] F.W. Walker, E.C. Ashby, J. Am. Chem. Soc. 91 (1969) 3845–3850.
[27] G.E. Parris, E.C. Ashby, J. Am. Chem. Soc. 93 (1971) 1206–1213.
[28] E.C. Ashby, G. Parris, F. Walker, Chem. Commun. (1969) 1464.
[29] T.D.W. Claridge, High-Resolution NMR Techniques in Organic Chemistry, Pergamon Press, Amsterdam, 1999.
[30] (a) S. Miertus, J. Tomasi, Chem. Phys. 65 (1982) 239–245;
(b) V. Barone, M. Cossi, J. Tomasi, J. Comput. Chem. 19 (1998) 404–417, and references cited therein.
[31] F. Ehrenberger, Quantitative Organische Elementaranalyse, VCH, Weinheim, 1991, pp. 555–556.
[32] Data obtained by PERCH Computer Software, University of Kuopio, Finland, 2000.
[33] G.M. Sheldrick, SHELXS-97, SHELXL-97: Programs for Crystal Structure Determination, University of Göttingen, Göttingen, Germany, 1990–1997.
[34] M.J. Frisch, G.W. Trucks, H.B. Schlegel, G.E. Scuseria, M.A. Robb, J.R. Cheeseman, V.G. Zakrzewski, J.A. Montgomery Jr., R.E. Stratmann, J.C. Burant, S. Dapprich, J.M. Millam, A.D. Daniels, K.N. Kudin, M.C. Strain, O. Farkas, J. Tomasi, V. Barone, M. Cossi, R. Cammi, B. Mennucci, C. Pomelli, C. Adamo, S. Clifford, J. Ochterski, G.A. Petersson, P.Y. Ayala, Q. Cui, K. Morokuma, D.K. Malick, A.D. Rabuck, K. Raghavachari, J.B. Foresman, J. Cioslowski, J.V. Ortiz, B.B. Stefanov, G. Liu, A. Liashenko, P. Piskorz, I. Komaromi, R. Gomperts, R.L. Martin, D.J. Fox, T. Keith, M.A. Al-Laham, C.Y. Peng, A. Nanayakkara, C. Gonzalez, M. Challacombe, P.M.W. Gill, B. Johnson, W. Chen, M.W. Wong, J.L. Andres, C. Gonzalez, M. Head-Gordon, E.S. Replogle, J.A. Pople, GAUSSIAN-98, Revision A.3, Gaussian, Inc., Pittsburgh, PA, 1998.
[35] (a) A.D. Becke, Phys. Rev. A 38 (1988) 3098–3100;
(b) A.D. Becke, J. Chem. Phys. 98 (1993) 5648–5652;
(c) C. Lee, W. Yang, R.G. Parr, Phys. Rev. B 37 (1988) 785–789;
(d) P.J. Stephens, F.J. Devlin, C.F. Chabalowski, M.J. Frisch, J. Phys. Chem. 98 (1994) 11623–11627.